



ELSEVIER

Available online at [www.sciencedirect.com](http://www.sciencedirect.com)

SCIENCE @ DIRECT®

Journal of Sound and Vibration 290 (2006) 388–409

JOURNAL OF  
SOUND AND  
VIBRATION

[www.elsevier.com/locate/jsvi](http://www.elsevier.com/locate/jsvi)

## Vibration analysis of the Second Saikai Bridge—a concrete filled tubular (CFT) arch bridge

Mistuhiko Yoshimura<sup>a</sup>, Qingxiong Wu<sup>b</sup>, Kazuo Takahashi<sup>b,\*</sup>,  
Shozo Nakamura<sup>b</sup>, Kazuyoshi Furukawa<sup>c</sup>

<sup>a</sup>*Nagasaki Shipyard & Machinery Works, Mitsubishi Heavy Industries, Ltd., 180, Akunoura-cho, Nagasaki, Japan*

<sup>b</sup>*Department of Civil Engineering, Faculty of Engineering, Nagasaki University, 1-14, Bunkyo-machi, Nagasaki, Japan*

<sup>c</sup>*Civil Engineering Information Office, Public Works Department, Nagasaki Prefectural Government, 2-13, Edo-machi, Nagasaki, Japan*

Received 30 April 2004; received in revised form 15 March 2005; accepted 2 April 2005

Available online 15 June 2005

---

### Abstract

Concrete-filled steel tubular (CFT) arch bridges have been rapidly developing in China since 1990. Research has focused on the static behavior, thermal stress and erection technique, however, and there has been very little research of natural vibrations and dynamic responses of these bridges. Japan's first CFT arch bridge in highway bridges, the Second Saikai Bridge, is now under construction in Nagasaki Prefecture. Furthermore, this bridge has a pedestrian bridge that is suspended under the girder, which is rare. Therefore, the natural vibration properties are examined, and the influence of pedestrian bridge structure on the natural vibration of main bridge is discussed first. Response analysis under a moving vehicle and pedestrian is carried out, and the response characteristics and response level are clarified. The natural vibrations and responses are compared to those of CFT arch bridges that have been constructed in China. Results show the fine performance of both main bridge and pedestrian bridge of the Second Saikai Bridge.

© 2005 Elsevier Ltd. All rights reserved.

---

\*Corresponding author. Tel.: +81 95 819 2610; fax: +81 95 819 2627.

E-mail address: [takahasi@civil.nagasaki-u.ac.jp](mailto:takahasi@civil.nagasaki-u.ac.jp) (K. Takahashi).

## 1. Introduction

In arch bridges, it may be practical to use concrete filled steel tubes (CFT) for the arch ribs in which the compression axial force is predominant. The infilled concrete delays local buckling of the steel tube, and the steel tube reinforces the concrete against tension, bending moment, and shear force. The tube also serves as a formwork for the concrete during construction of the bridge, thus saving a major construction cost [1,2]. Moreover, the composite structural action between the infilled concrete and the steel tube improves the member's load-carrying capacity. As a result of these advantages, CFT construction for bridges has become widespread in recent decades [3,4]. More than one hundred CFT arch bridges have been constructed since 1990 [5–7] in China, and a CFT arch bridge with the span length of over 400 m is now being constructed [8]. The Second Saikai Bridge, the first CFT arch highway bridge in Japan, is under construction in Nagasaki Prefecture.

Research into CFT arch bridges has focused on the static behavior, thermal stress and erection technique [7]. However, there has been very little research into vibrations and seismic responses of CFT arch bridges. The dynamic properties of CFT arch bridges have not been examined in detail. Therefore, it is necessary to evaluate the characteristics of the natural vibration, the dynamic response under traffic loading and the nonlinear seismic response of the actual Second Saikai Bridge. This paper focuses on the in-plane vibrations and discusses the properties of the natural vibration and the traffic-induced vibration. The nonlinear seismic responses of this bridge were discussed in a separate paper [9].

This bridge has a pedestrian bridge under the girder. The pedestrian bridge allows pedestrians to cross the Second Saikai Bridge and visit a nearby public park. There is no other example in a highway bridge with such a structure suspended under the girder so it is necessary to understand the dynamic response characteristics of the pedestrian bridge. In particular, the response levels of the pedestrian bridge when a vehicle passes over the girder or when a pedestrian walks on the pedestrian bridge must be understood.

In this paper, the in-plane natural vibration properties of the bridge and the pedestrian bridge are examined, and the influence of the pedestrian bridge structure on the natural vibration of the bridge is discussed first. A response analysis induced by a moving vehicle is carried out, and the response characteristics of the bridge and the pedestrian bridge are clarified. The natural vibrations and responses are compared to those of CFT arch bridges that have been constructed in China. Finally, the response induced by a pedestrian walking on the pedestrian bridge is evaluated.

## 2. A brief description of the Second Saikai Bridge

The Second Saikai Bridge (tentative name) is a highway bridge on the Nishisonogi Region Expressway. The bridge crosses the Harioseto channel and connects the Sasebo urban area and the Nagasaki urban area. The bridge is scheduled to be completed in 2006. As shown in Fig. 1(a), the main span is 240 m in length and the side spans are 30 m in length. The bridge is 20.2 m in width. The landscape of the site, the need to harmonize the design with that of the present Saikai Bridge (a deck type steel arch bridge with a span of 216 m, completed in 1955) and the need to

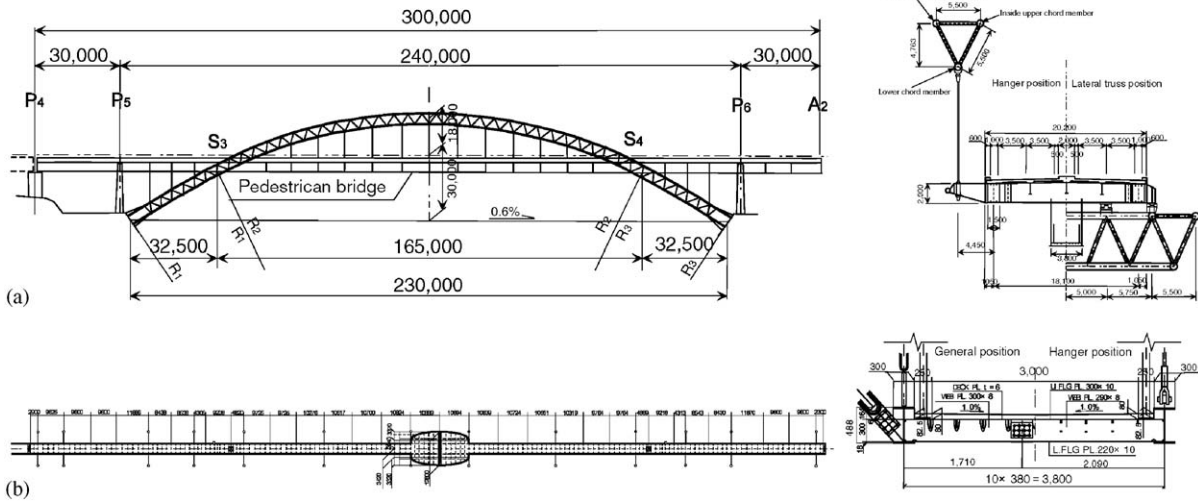


Fig. 1. General view of the Second Saikai Bridge (unit: mm). (a) Main bridge; (b) Pedestrian bridge.

reduce the bridge's construction costs together lead the selection of the half-through braced-rib CFT arch bridge design for the main span. The bridge has two parallel arch ribs, each of which has a triangular cross-section consisting of three steel tubes. High fluidity concrete fills the three steel tubes. The three steel tubes have an outer diameter of 812.8 mm and a thickness that differs depending upon the position of the arch rib. The deck system consists of I-beams arranged longitudinally, upon which a composite slab is placed.

There is a pedestrian bridge under the bridge, which allows pedestrians to cross the Second Saikai Bridge and visit the public park since the sidewalk cannot be built in the highway bridge. This pedestrian bridge is 293.225 m long and 3 m wide. The pedestrian bridge itself has a girder made of two H-type beams. This girder hangs by strand rope and steel tube from the lateral beams of the bridge. A general view of the pedestrian bridge is shown in Fig. 1(b). The center of the pedestrian bridge has been widened to allow visitors to enjoy the view from the Second Saikai Bridge.

The pedestrian bridge is designed by using static sidewalk live load specified in Design Specifications for Highway Bridges in Japan [10]. The dynamic design considering moving vehicles and walking pedestrians is not adopted in Design Specifications for Highway Bridges in Japan. Therefore, the dynamic analysis is performed to check the dynamic safety of the bridge.

### 3. Analytical model

#### 3.1. Basic assumptions

The basic assumptions of the present paper are as follows:

- (1) The geometric nonlinearity is not considered to evaluate the response characteristics of this bridge under a moving vehicle or pedestrian traffic.

- (2) It is assumed that the stress–strain relationships of steel tube and filled concrete are linear. The deformation of steel tube is taken equal to that of filled concrete along the boundary of two materials. Consequently, the slip between steel tube and filled concrete does not occur.
- (3) Equations of bridge–single-vehicle dynamic system subjected to road roughness are used to evaluate the responses of main bridge and the pedestrian bridge. A two-degrees-of-freedom vehicle model is employed. The model of road surface is modeled by a Gaussian process.

### 3.2. Integrated bridge model

Fig. 2 shows a three-dimensional FE model of the integrated bridge. This model takes into account the rigidity and mass of the pedestrian bridge. The arch rib, stiffening girder, lateral bracing, and pier are all modeled using three-dimensional beam elements based on actual cross-sectional properties. The column and hanger are modeled using three-dimensional truss elements. The lumped mass matrix is adopted for this analysis.

On the pedestrian bridge, the girder and lateral beams of the pedestrian bridge are modeled using three-dimensional beam elements. The strand ropes and steel tubes are modeled using three-dimensional truss elements. The girder of the pedestrian bridge takes into account the stiffness of the floor system of pedestrian bridge.

The material properties of this CFT arch bridge (cross-sectional area  $A$  and elastic modulus  $E$ ), including the pedestrian bridge, are described in Table 1. Because the cross sections of the arch rib, stiffening girder or etc. are different depending upon the position, Table 1 shows the basic material properties at the center of those structures. The mass properties of the CFT arch rib bridge and the pedestrian bridge are summarized in Table 2.

Regarding boundary conditions, the springing position of the arch rib and the pier bases are fixed in all degrees of freedom. The earthquake shear force distribution rubber bearings are installed in the joints between the stiffening girder and the piers ( $P_4$ ,  $P_5$  and  $P_6$ ), the joints between the stiffening girder and abutment  $A_2$ , and the joints between the stiffening girder and the lateral beams ( $S_3$  and  $S_4$ ). The model uses linear springs to simulate these bearings. The points linking the suspension members of the pedestrian bridge and the stiffening girder of the bridge have the same

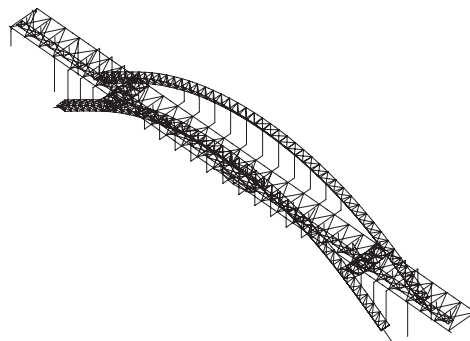


Fig. 2. Integrated bridge model.

Table 1  
Basic cross-sectional area  $A$  and elastic modulus  $E$  of the Second Saikai Bridge

Content		$A$ (m <sup>2</sup> )	$E$ (kN/m <sup>2</sup> )
Main bridge	Arch rib	$8.351 \times 10^{-2}$ (Inside, outside rib) $1.537 \times 10^{-2}$ (Lower rib)	$2.00 \times 10^8$
	Stiffening girder	$1.164 \times 10^{-1}$	$2.00 \times 10^8$
Pedestrian bridge	Hanger	$5.810 \times 10^{-3}$	$1.96 \times 10^8$
	Girder	$1.577 \times 10^{-2}$ (General part)	$2.00 \times 10^8$
		$1.803 \times 10^{-2}$ (Widened part)	
	Hanger	$9.898 \times 10^{-4}$ (Cable)	$1.40 \times 10^8$
$4.078 \times 10^{-3}$ (Steel tube)		$2.00 \times 10^8$	

Table 2  
Mass properties of the Second Saikai Bridge

Content		Weight (kN)
Main bridge	Arch rib	24,604
	Stiffening girder	7,747
	Floor slab	56,050
	Lateral bracing etc.	11,139
Pedestrian bridge girder		5,858

longitudinal, vertical and out-of-plane displacements as the stiffening girder of the main bridge. The vertical displacements in the original points and the end points of the pedestrian bridge are restrained, as to the out-of-plane displacements in the lateral bracing of the pedestrian bridge.

### 3.3. Original bridge model and separate pedestrian bridge model

In order to examine the influence of the pedestrian bridge on the natural vibrations of the bridge, the original bridge model and a separate pedestrian bridge model are used in addition to the integrated bridge model.

In the original bridge model in Fig. 3(a), the rigidities of the pedestrian bridge are not taken into account, and the masses of the pedestrian bridge are included with those of the girder. This original bridge model is adopted for the nonlinear seismic analysis of the main bridge.

The separate pedestrian bridge model is shown in Fig. 3(b). In this model, only the pedestrian bridge's structure is considered. Regarding the boundary condition of the pedestrian bridge model, the points that link the hangers of the pedestrian bridge and the stiffening girder of the bridge are fixed in the longitudinal, vertical and out-of-plane degrees of freedom.

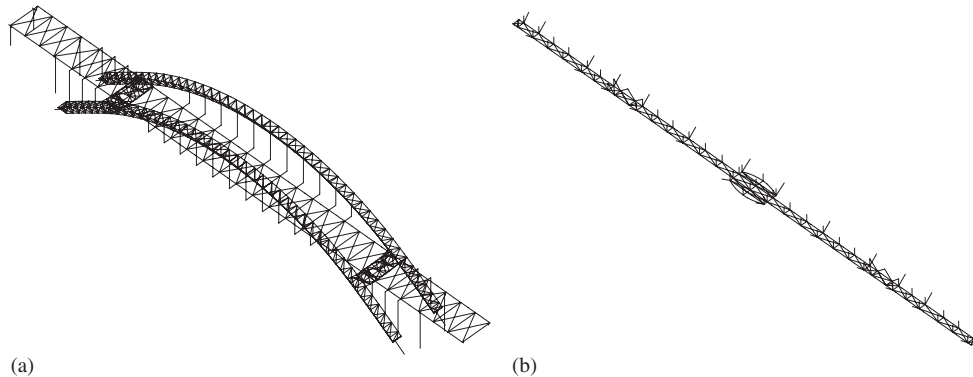


Fig. 3. (a) Original bridge model and (b) separate pedestrian bridge model.

#### 4. Natural vibration characteristics

The natural vibration analysis is carried out using the integrated bridge model, and the natural vibration characteristics are examined. In this paper, the natural vibrations of the bridge except for the local oscillation of the pedestrian bridge are called the ‘*natural vibrations of the main bridge*’, and the local natural vibrations of the pedestrian bridge are called the ‘*natural vibrations of the pedestrian bridge*’.

##### 4.1. Natural vibration characteristics of main bridge

The natural frequencies and modal shapes of the in-plane natural vibrations of the main bridge are demonstrated in Table 3.



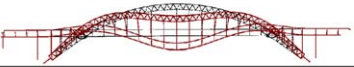











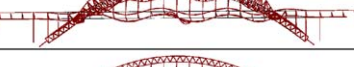
The first in-plane natural vibration, which has a frequency of 0.472 Hz, corresponds to the floating mode, as it does with cable-stayed bridges. This mode is a longitudinal pendulum-like movement of the stiffening girder as illustrated in Table 3. This is due to the rubber bearings installed in the longitudinal direction of the bridge that distribute earthquake shear forces. The second in-plane natural vibration has a frequency of 0.639 Hz, which corresponds to the unique antisymmetric mode of arch bridges.

Furthermore, there are in-plane natural vibration modes in which the vibrations of the side spans are predominant. They have natural frequencies of 2.553 Hz (the 13th mode) and 2.644 Hz (the 15th mode).

##### 4.2. Natural vibration characteristics of pedestrian bridge

Table 4(a) shows in-plane natural vibrations of the pedestrian bridge using the integrated bridge model. The lowest in-plane natural frequency of the pedestrian bridge natural vibration is 2.276 Hz, which is much higher than the lowest in-plane natural frequency of the natural vibration of the main bridge.

Table 3  
In plane natural vibrations of the main bridge


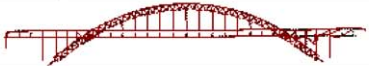
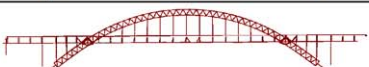
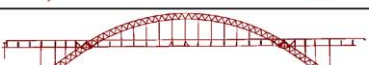
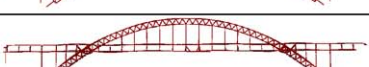
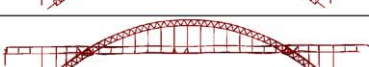










No.	Freq. (Hz)	Modal shape
1	0.472	
2	0.639	
3	0.929	
4	1.474	
5	1.509	
6	1.948	
7	2.025	
12	2.512	
13	2.553	
14	2.631	
15	2.644	
18	2.856	
19	2.909	
20	2.979	
24	3.285	

#### 4.3. Influence of natural vibrations of pedestrian bridge on natural vibrations of main bridge

The weight of the pedestrian bridge on the Second Saikai Bridge is 8% of the steel weight of the integrated bridge. Therefore, in the model of the integrated bridge, the original bridge and the pedestrian bridge are treated as a monolithic structure. However, the original bridge is used for



Table 4  
In-plane natural vibrations of the pedestrian bridge

No.	Freq. (Hz)	Modal shape
(a) Integrated bridge model		
8	2.276	
9	2.285	
10	2.367	
11	2.383	
16	2.716	
17	2.733	
21	3.017	
22	3.147	
(b) Separate pedestrian bridge model		
1	2.276	
2	2.285	
3	2.367	
4	2.383	
5	2.716	
6	2.733	
7	3.017	
8	3.147	

the seismic analysis of the main bridge [9] and the separate pedestrian bridge model is used for the natural vibration analysis of the pedestrian bridge itself. In other words, it is assumed that the effect of the rigidity of the pedestrian bridge on the vibration of the main bridge is negligible.



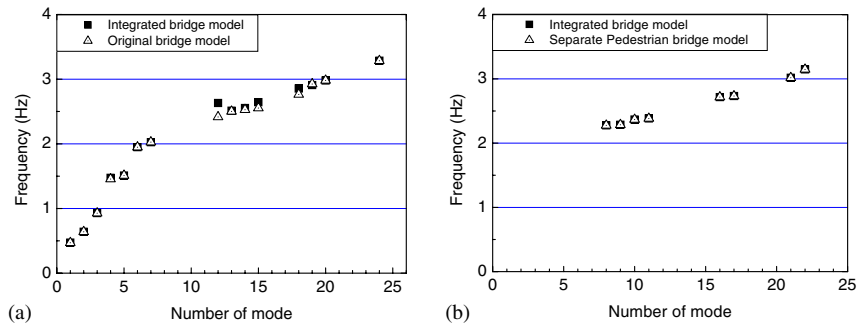


Fig. 4. In-plane natural frequencies: (a) natural vibrations of the main bridge; (b) natural vibrations of the pedestrian bridge.

The influence of the natural vibrations of the pedestrian bridge on the natural vibrations of the integrated bridge is considered using the integrated bridge, original bridge, and independent pedestrian bridge models in order to analyze the validity of the assumptions.

The in-plane natural frequencies of the main bridge vibrations using the integrated bridge model and the original bridge model are plotted in Fig. 4(a). There are some differences in the natural modes near the natural frequency of 2.5–2.8 Hz, though the results using the original bridge model coincide with those using the whole bridge model. The vertical displacements in the origin points and the end points of the pedestrian bridge in the integrated bridge model are restrained, but these boundary conditions are not applied to the original bridge model. In other words, the differences in the natural frequencies are due to the different boundary conditions. The natural frequency of the original bridge model is about 8% lower than that of the integrated bridge model. Therefore, the influence of the natural vibrations of the pedestrian bridge on the natural vibration of the main bridge is seen to be small.

Fig. 4(b) and Table 4 show the natural vibrations of the pedestrian bridge for the integrated bridge model and for the separate pedestrian bridge model. The natural frequencies of the separate pedestrian bridge model agree well with those for the integrated bridge model. According to the dense distribution of natural frequencies of the separate pedestrian bridge, the vibration behavior of the pedestrian bridge installed in the main bridge is similar to that of an attached beam connected with a main beam by uniformly elastic spring. Thus, the effect of the rigidity of the pedestrian bridge on the vibration of the main bridge is negligible. Moreover, the natural vibrations of the pedestrian bridge can be evaluated using the separate pedestrian bridge model. However, when a moving vehicle passes by the girder of the main bridge, the dynamic analysis of the pedestrian bridge must use the integrated bridge model.

#### 4.4. Comparison of CFT arch bridge and steel arch bridge

The Jiangnan Wuqiao Bridge (240 m, CFT, China) [11] and the Saikai Bridge (216 m, steel, Japan) [12], which have almost the same span length as the Second Saikai Bridge, are used to compare the natural vibration properties of CFT arch bridges with those of steel arch bridges. The in-plane natural frequencies of those three bridges are summarized in Table 5. The weigh of CFT

Table 5  
Natural frequencies of CFT arch bridges and steel arch bridge

Bridge name	Span (m)	Type	Natural frequencies of in-plane modes (Hz)			
			First antisymmetric	First symmetric	Second antisymmetric	Second symmetric
Second Saikai Bridge	230	CFT	0.639	0.929	1.509	1.474
Jiangnan Wuqiao Bridge	240	CFT	0.724	1.229	1.878	2.041
Saikai Bridge	216	Steel	1.153	1.507	2.805	2.306

arch bridges is greater than that of the steel arch bridge. Therefore, the natural frequencies of the CFT arch bridges are smaller than those of steel bridges as can be seen in Table 5. The arch action is not effective in the out-of-plane direction. The seismic safety of CFT arch bridges should be checked when the bridges are subjected to earthquake in the out-of-plane direction [9–13].

### 5. Response characteristics under a moving vehicle

In this section, the vibrations of the Second Saikai Bridge under traffic loading are examined using the bridge–vehicle–road surface model based on Refs. [14–16]. For a long-span bridge, there are often multiple vehicles traveling on it. The response level of bridge subjected to multiple vehicles becomes large. However, the case where a single vehicle is traveling the bridge has the large frequency in which a pedestrian receives the influence of traveling vehicle. Accordingly, in the present paper study, a single moving vehicle is adopted to evaluate the response level of this bridge.

The equations of motion of the bridge subjected to the loading can be expressed as

$$[M]\{\ddot{y}_g\} + [C]\{\dot{y}_g\} + [K]\{y_g\} = \{F\}, \tag{1}$$

where  $[M]$ ,  $[C]$  and  $[K]$  are the mass, damping and stiffness matrices of the bridge, respectively,  $\{F\}$  is the load vector,  $\{y_g\}$  is the displacement vector representing the displaced shape of the bridge,  $\{\dot{y}_g\}$  is the velocity vector and  $\{\ddot{y}_g\}$  is the acceleration vector [17].

A two-degrees-of-freedom vehicle is used as shown in Fig. 5 and the equation of motion of vehicle is

$$[M_v]\ddot{Z}_{t+\Delta t} + [C_v]\dot{Z}_{t+\Delta t} + [K_v]Z_{t+\Delta t} = \{F_v\} \tag{2}$$

and the force from vehicle to bridge  $\{F\}$  is expressed as follows

$$\{F\} = -\varphi\{F_v\}, \tag{3}$$

where

$$[M_v] = \begin{bmatrix} M_S & \\ & M_\theta \end{bmatrix}, \quad [C_v] = \begin{bmatrix} C_{S1} + C_{S2} & r_1 C_{S1} - r_2 C_{S2} \\ r_1 C_{S1} - r_2 C_{S2} & r_1^2 C_{S1} + r_2^2 C_{S2} \end{bmatrix}$$

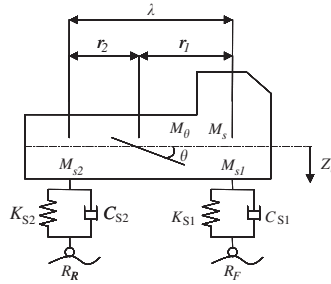


Fig. 5. Two-degrees-of-freedom vehicle model.

Table 6  
Parameters of vehicle

$M_S$ (t)	25.000
$M_\theta$ (t m <sup>2</sup> )	64.000
$M_{S1}$ (t)	5.000
$M_{S2}$ (t)	20.000
$K_{S1}$ (kN/m)	1776.529
$K_{S2}$ (kN/m)	7106.115
$C_{S1}$ (kN s/m)	28.274
$C_{S2}$ (kN s/m)	113.097
$r_1$ (m)	3.200
$r_2$ (m)	0.800
Damping constant $h_c$	0.030
First frequency (Hz)	3.000
Second frequency (Hz)	3.000

and

$$[K_v] = \begin{bmatrix} K_{S1} + K_{S2} & r_1 K_{S1} - r_2 K_{S2} \\ r_1 K_{S1} - r_2 K_{S2} & r_1^2 K_{S1} + r_2^2 K_{S2} \end{bmatrix}$$

are the mass, damping and stiffness matrices of the vehicle,  $\{\ddot{Z}\}$ ,  $\{\dot{Z}\}$  and  $\{Z\}$  are the acceleration, velocity and displacement vectors of the vehicle and  $Z = \begin{Bmatrix} Z_s \\ \theta \end{Bmatrix}$ ,  $\varphi$  is the coefficient matrix which convert the load to the node load of the bridge,  $\{F_v\}$  is the load vector subjected to vehicle and is expressed as

$$\begin{aligned} \{F_v\} = & \begin{bmatrix} C_{S1} & C_{S2} \\ r_1 C_{S1} & -r_2 C_{S2} \end{bmatrix} \begin{Bmatrix} \dot{R}_F \\ \dot{R}_R \end{Bmatrix} + \begin{bmatrix} K_{S1} & K_{S2} \\ r_1 K_{S1} & -r_2 K_{S2} \end{bmatrix} \begin{Bmatrix} R_F \\ R_R \end{Bmatrix} \\ & + \begin{bmatrix} C_{S1} & C_{S2} \\ r_1 C_{S1} & -r_2 C_{S2} \end{bmatrix} \begin{Bmatrix} \dot{y}_F \\ \dot{y}_R \end{Bmatrix} + \begin{bmatrix} K_{S1} & K_{S2} \\ r_1 K_{S1} & -r_2 K_{S2} \end{bmatrix} \begin{Bmatrix} y_F \\ y_R \end{Bmatrix}. \end{aligned} \quad (4)$$

$y_F$  and  $y_R$  are the displacements of the girder at the positions of the front and rear wheel.  $R_F$  and  $R_R$  are the road surface roughness at the position of the front and rear wheel. The parameters of

the vehicle used in this paper are listed in Table 6. The power spectral density of the road surface roughness is determined using Refs. [14–16] and can be expressed as

$$S_r(\Omega) = \frac{A}{\Omega^2 + a^2}, \tag{5}$$

where  $\Omega$  is the frequency of the road surface (cycle/m),  $A$  is a parameter expressing the level of road surface roughness and  $a$  is a parameter based on the observed result. In the present paper, the road surface is assumed to be in the best condition when  $A = 0.001$  and  $a = 0.05$ . Just for reference, a simulated wave of road surface roughness by AR model [18] is presented in Fig. 6. According to ISO standard [19], the wave corresponds to the ‘best’ road surface ( $A = 0.001$ ). Fig. 7 shows the power spectral density of this wave and the target spectral density. The power spectral density of the simulated wave coincides with the target power spectral density.

The response of the bridge under a moving vehicle is obtained by solving Eqs. (1)–(3). The Newmark  $\beta$  method ( $\beta = 0.25$ ) of direct integration is used.

The Rayleigh damping [20] is used to form the damping matrix of bridge  $[C]$  as a linear combination of mass matrix  $[M]$  and stiffness matrix  $[K]$  (see Eq. 1)

$$[C] = a_3[M] + a_4[K], \tag{6}$$

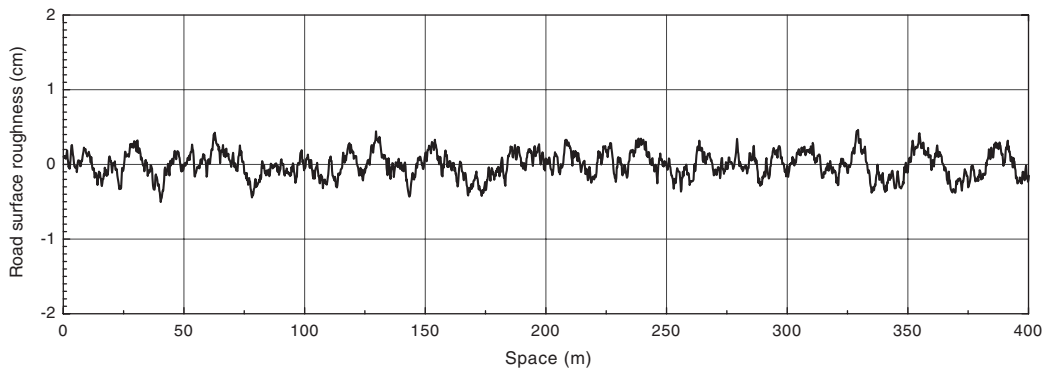


Fig. 6. Road surface roughness.

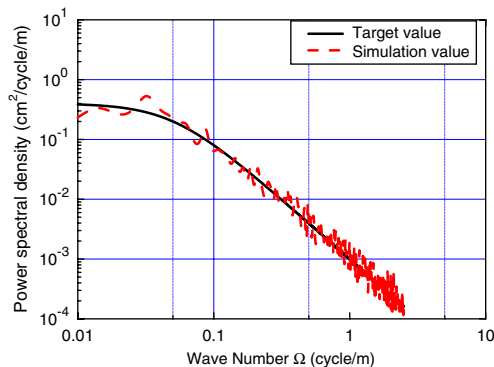


Fig. 7. Power spectrum of road surface roughness.

in which  $a_3$  and  $a_4$  are arbitrary proportional factors. These factors are given in terms of two different frequencies ( $\omega_i, \omega_j$ ) and the corresponding critical damping ratios ( $h_i, h_j$ ) ( $i < j$ ) and expressed as

$$a_3 \frac{2f_i f_j (h_i/2\pi f_j - h_j/2\pi f_i)}{f_j^2 - f_i^2}, \quad a_4 \frac{2(h_j f_j/2\pi - h_i f_i/2\pi)}{f_j^2 - f_i^2}. \tag{7}$$

In this paper, the damping constants  $h_i$  and  $h_j$  are assumed to be equal to 0.01 and the frequencies  $f_i$  and  $f_j$  are set to 0.639 Hz and 0.929 Hz, respectively.

5.1. Response characteristics of girder

Fig. 8 shows the maximum velocities of the girder and arch rib when a vehicle passes by the girder of the main bridge at a speed of 80 km/h. The vertical axis corresponds to the maximum velocities and the horizontal axis corresponds to the coordinate in the longitudinal direction of the bridge.

On the main span, the maximum velocity of the girder of the main span is about 0.8 cm/s.

There is an investigation for the response level of a CFT arch bridge built in China [21]. The Shitanxi Bridge is a half-through CFT arch with a span length of 136 m. The bridge has two parallel arch ribs, each of which has a rectangular cross-section consisting of four steel tubes. The

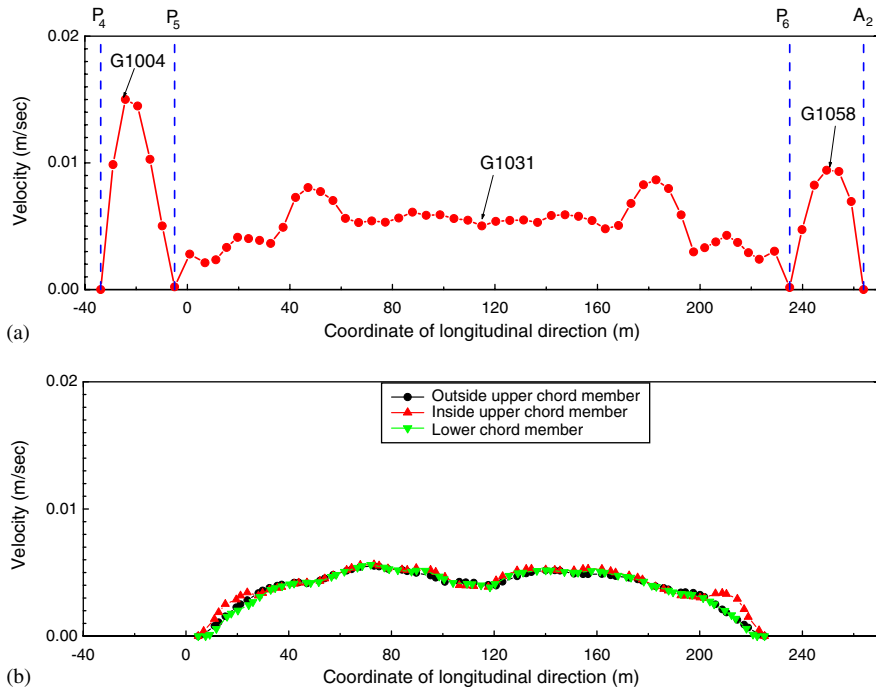


Fig. 8. Maximum velocities under moving vehicle: (a) girder; (b) arch rib.

response level of this bridge under the vehicle loading is investigated in 2000. The maximum velocity of the girder in the Shitanxi Bridge is about 5.7 cm/s.

Comparing the maximum velocity of the Second Saikai Bridge with that of the Shitanxi Bridge, the vibration level in the girder of the main span of the Second Saikai Bridge under traffic loading is smaller than that of the Shitanxi Bridge.

The maximum velocity in the arch rib of the Second Saikai Bridge is less than 0.5 cm/s as shown in Fig. 8(b), while that of the Shitanxi Bridge is about 3.9 cm/s. Therefore, the vibration level in the arch rib of the Second Saikai Bridge is smaller than that of the Shitanxi Bridge.

However, a vibration with a maximum velocity of 1.5 cm/s is generated in the side spans, which have a span length of 30 m. Time histories of displacement, velocity and acceleration at the center points (G1004 and G1058) of the side spans are shown in Fig. 9. When a vehicle passes by the center point of the side span ( $t = 0.79$  s), the displacement of the center point G1004 of the side span is the largest. The displacement of the girder at  $t = 0.79$  s is shown in Fig. 10. The girder in the main span generates small displacements even if the displacement of the side span is predominant. In other words, the vibration of the side span is local, and the in-plane natural vibration, in which the vibration of the side span with natural frequency of 2.553 Hz (the 13th mode in Table 3) is predominant, is induced. This means that the response of the side span is large due to the resonance, since the in-plane natural frequency of 2.553 Hz in the side spans corresponds with the natural frequency of 3.0 Hz of the vehicle.

### 5.2. Response characteristics of pedestrian bridge

Fig. 11 shows the maximum velocities of the pedestrian bridge when a vehicle passes by the girder of the main bridge at a speed of 80 km/h. Fig. 12 shows the time histories for center points P21009 and P21109 of the side spans. Fig. 13 shows the time histories for center points P21057 of the main span. The maximum velocity of the main span is about 0.8 cm/s and that of side spans is about 1.8 cm/s, which are the same as those of the girder of the main bridge.

The fundamental vibration frequency of the added pedestrian bridge is much higher than that of the main bridge so that the added pedestrian bridge does not behave like a tuned mass damper in the present bridge.

### 5.3. Response level

The ergonomic evaluation method developed by Kobori and Kajikawa [22] is used to appraise the vibration sensibility of the traffic-induced vibration on the Second Saikai Bridge. The vibration stimulation  $S$  (cm/s) is calculated using the effective value of the maximum velocity  $V_{\max}$  (cm/s). It is described by the following equation:

$$S = V_{\max} / \sqrt{2}. \quad (8)$$

The vibration greatness level VGL(dB) is given as described by the following equation:

$$\text{VGL} = 20 \log_{10}(S/S_0) \quad (S_0 = 1.4 \times 10^{-2} \text{ cm/s}). \quad (9)$$

The vibration greatness VG can then be obtained from the following expressions:

$$\log_{10} \text{VG} = 0.05(\text{VGL} - 40) \text{ when } \text{VGL} \leq 40 \text{ dB},$$

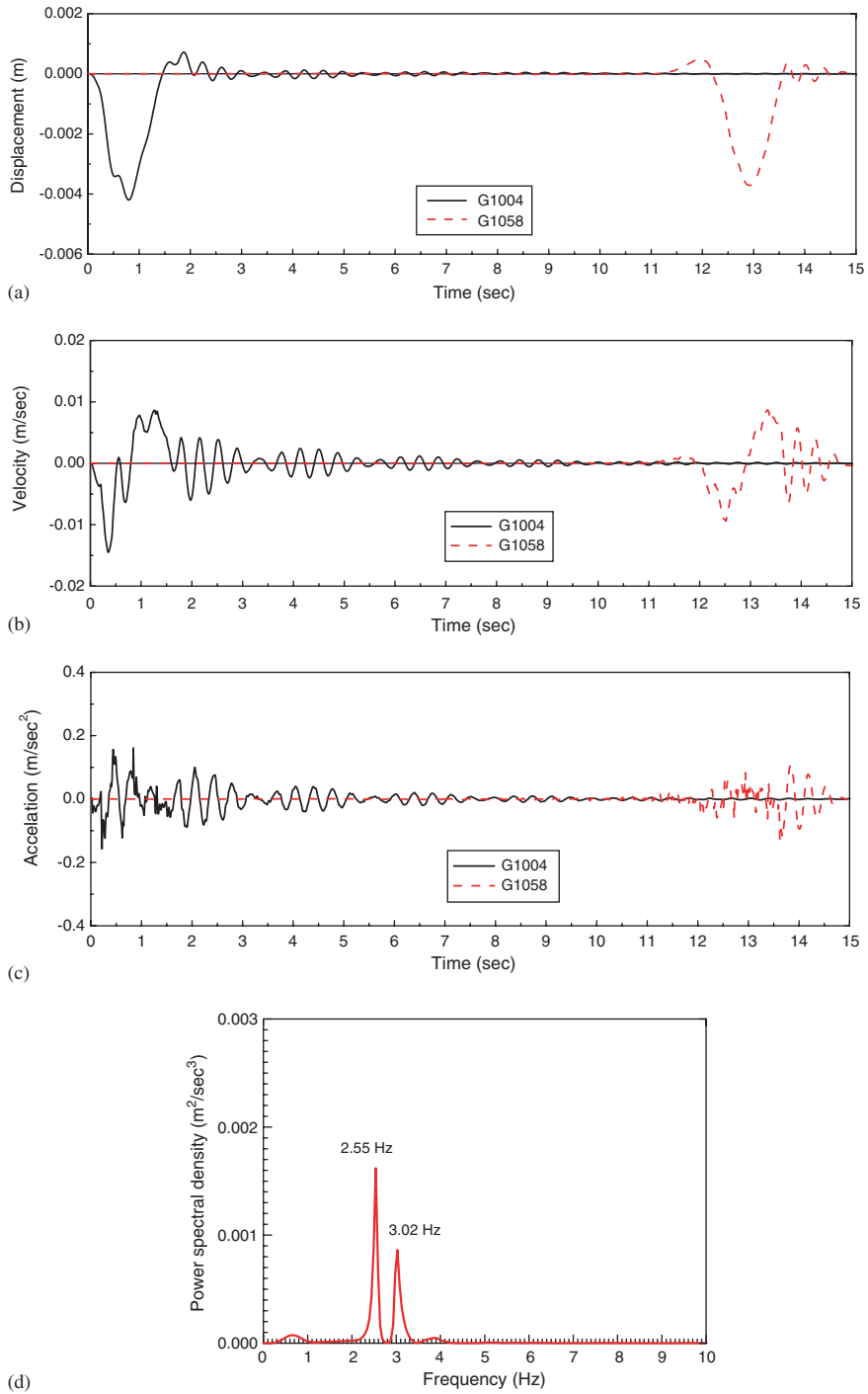


Fig. 9. Time histories at the center point of side span (G1004 and G1058): (a) displacement; (b) velocity; (c) acceleration; (d) power spectral density of G1004 acceleration.



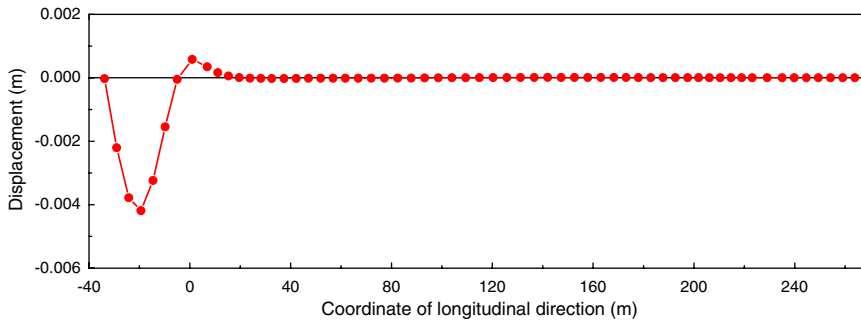


Fig. 10. Displacement of the girder at  $t = 0.79$  s.

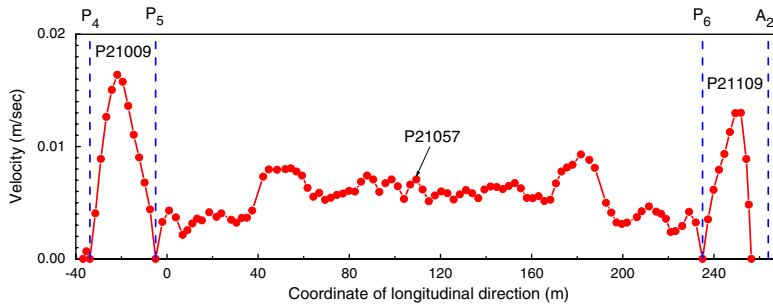


Fig. 11. Maximum velocities of pedestrian bridge under moving vehicle.

$$\log_{10} VG = 0.03(VGL - 40) \text{ when } VGL > 40 \text{ dB.} \tag{10}$$

The relationship between the category and the lower limit of the VG for pedestrians is shown in Table 7.

Table 8 summarizes the maximum velocities and corresponding VG of the Second Saikai Bridge.

Regarding the main span, both the maximum velocity of the girder and that of the pedestrian bridge are about 0.014m/s, which is equal to  $VG = 0.73$ . From the viewpoint of vibration sensation, its VG is in the category of ‘definitely perceptible’, and the vibration of the main span under traffic loading is small.

In the side spans, the maximum velocity of the girder of the main bridge and that of the pedestrian bridge are about 0.016m/s and 0.013 m/s, which are equal to  $VG = 0.80$  and  $VG = 0.66$ , respectively. These VG are in the category of ‘definitely perceptible’. Therefore, the vibration of the side spans under traffic loading is small, too.

### 6. Response characteristics under pedestrian traffic

The lowest natural frequency of the pedestrian bridge is 2.276 Hz. This is close to 2.0 steps/s, which corresponds to the pace of an adult walking down a street [23]. There is some apprehension

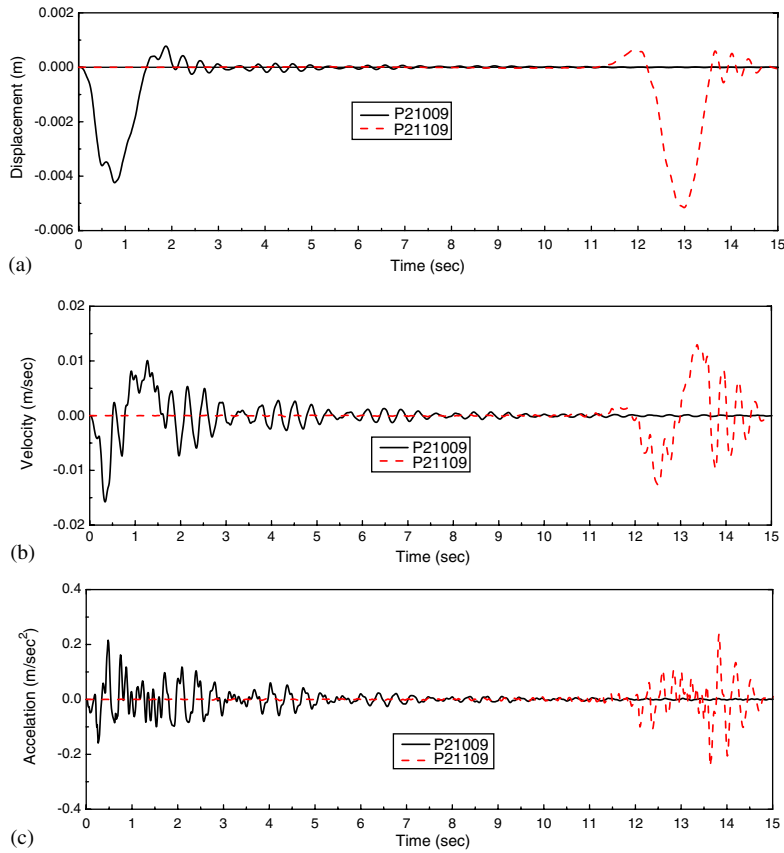


Fig. 12. Time histories of points (P21009 and P21109) in the pedestrian bridge: (a) displacement; (b) velocity; (c) acceleration.

about the resonance induced by a pedestrian walking on the pedestrian bridge when the predominant frequency of the pedestrian bridge is near the pace of the pedestrian. Accordingly, the dynamic response characteristics of the pedestrian bridge induced by pedestrian traffic are examined.

### 6.1. Load induced by pedestrian

The following walking load, which takes into account the dead load of the pedestrian [23,24], is used to examine the dynamic response characteristics that are induced by a pedestrian walking on the pedestrian bridge.

$$F(t) = W(1 + \alpha \cos \omega t), \quad (11)$$

where  $W$  is the weight of the pedestrian and is set to 0.588 kN (60 kgf) in this paper,  $\omega = 2\pi f$  is the circular frequency of the pace,  $\alpha$  is the ratio of the impulsive force according to the pace and the relationship between  $\alpha$  and pace is shown in Fig. 14 according to Ref. [23]. The relationship between velocity and pace is also shown in the same figure.

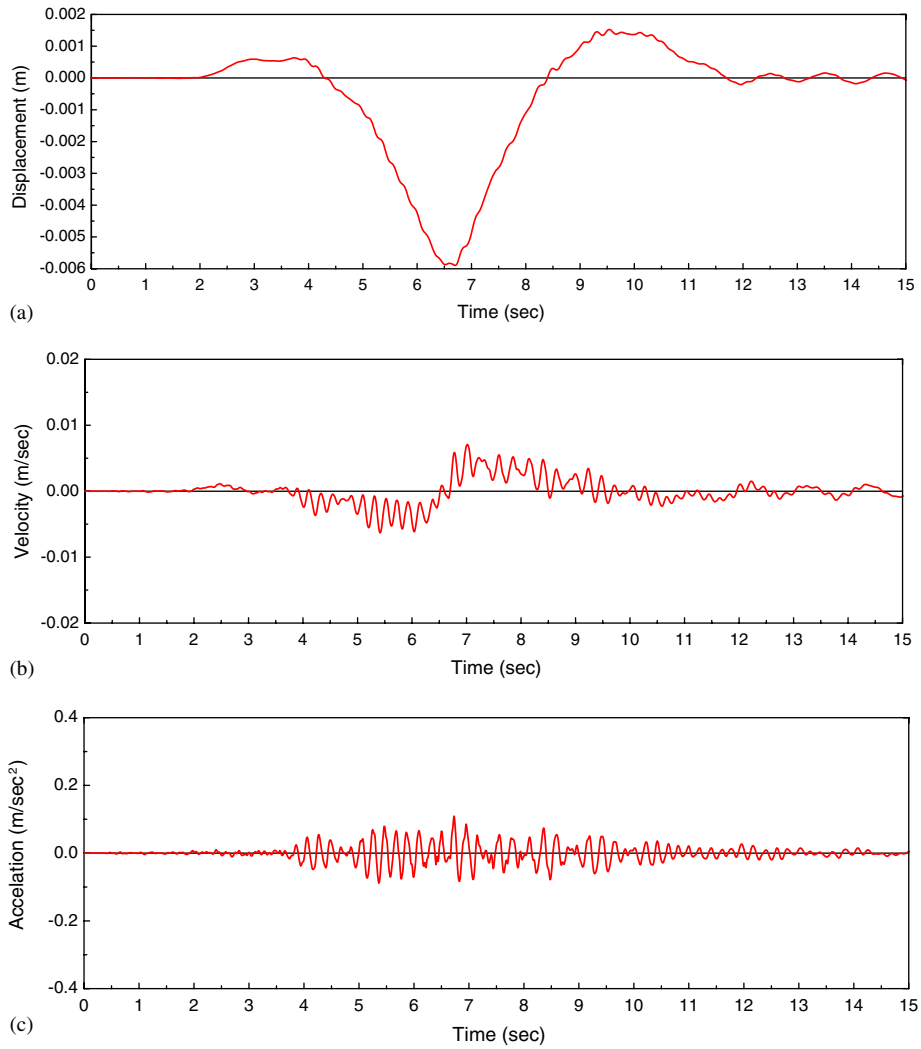


Fig. 13. Time histories of point P21057 in the pedestrian bridge: (a) displacement; (b) velocity; (c) acceleration.

Table 7  
Category and lower limit of VG for pedestrian

No.	Content of category	VG
1	Slightly perceptible	0.32
2	Definitely perceptible	0.61
3	Lightly hard to walk	1.12
4	Extremely hard to walk	1.48

Table 8  
Response level of the Second Saikai Bridge

Position		$V_{\max}$ (m/s)	VG	Category
Girder	N1004	0.01449	<b>0.73</b>	Definitely perceptible
	N1031	0.00502	0.25	—
	N1058	0.00942	0.48	Slightly perceptible
Pedestrian bridge	N21009	0.01577	<b>0.80</b>	Definitely perceptible
	N21057	0.00707	0.36	Slightly perceptible
	N21109	0.01297	<b>0.66</b>	Definitely perceptible

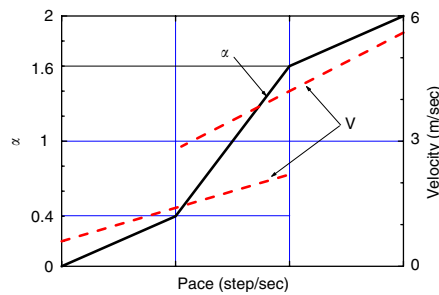


Fig. 14. Relationship between  $\alpha$  and  $v$  [23].

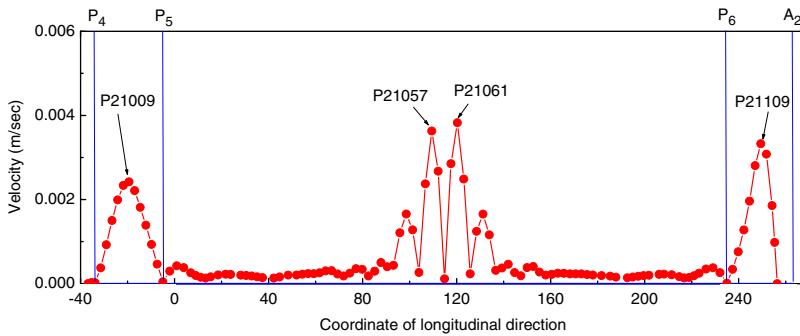


Fig. 15. Maximum velocity of the pedestrian bridge in the pace of 2.55 steps/s.

### 6.2. Response characteristics of pedestrian bridge

The maximum velocities of the pedestrian bridge at the pace of 2.55 steps/s are shown in Fig. 15. Among all the points shown, the largest velocities are generated at the center point P21009 of the side span between pier P<sub>4</sub> and pier P<sub>5</sub>, at center point P21109 of the side span between pier P<sub>6</sub> and abutment A<sub>2</sub>, and at points P21057 and P21061 in the wide part of the main span.

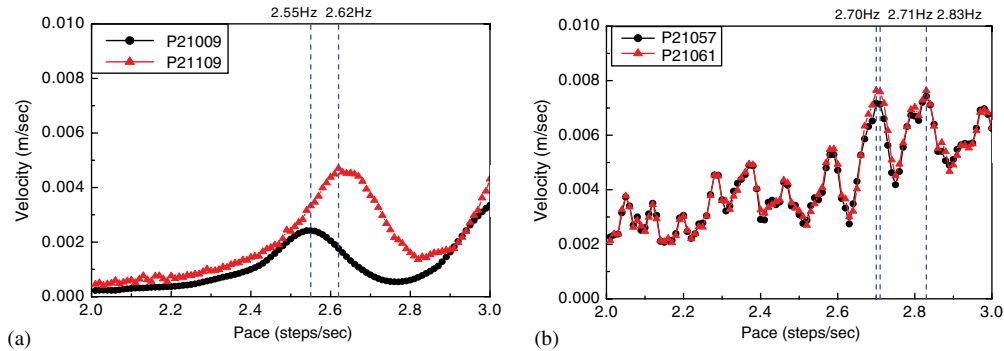


Fig. 16. Relationship between the velocity and the pace of pedestrian: (a) center point of side spans; (b) wide part.

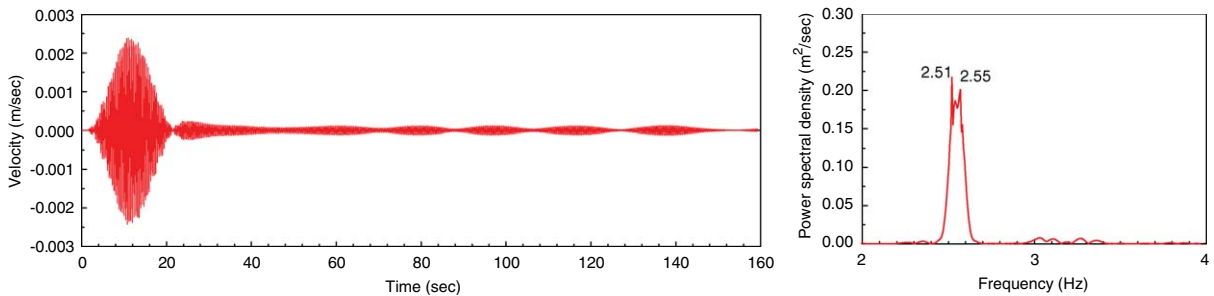


Fig. 17. Time history of velocity and power spectrum of P21009 in the pace of 2.55 steps/s.

The relationship between the pace of a walking pedestrian and the velocity at those four points is shown in Fig. 16.

Regarding point P21009, shown in Fig. 16(a), the peak of maximum velocity appears near 2.55 steps/s. Fig. 17 shows the time history of the velocity and the power spectrum at the pace. The power spectrum indicates that the frequencies of 2.51 and 2.55 Hz are predominant. 2.51 Hz corresponds to the natural frequency of the 12th vibration mode of the main bridge (see Table 3), and 2.55 Hz corresponds to the natural frequency of the 13th vibration mode of the main bridge (see Table 3) and the frequency of the pedestrian's pace. In other words, a pace of 2.55 steps/s induces vibrations at the frequencies of the 12th and 13th modes of the main bridge.

The peaks of the maximum velocities of points P21057 and P21061 in the main span appear near 2.70, 2.71 and 2.83 steps/s, as shown in Fig. 13(b). In the response spectrum shown in Fig. 18, the frequencies of 2.72 and 2.67 Hz are predominant. The frequency of 2.72 Hz corresponds to the natural frequency of the 16th mode of the pedestrian bridge (see Table 4), and the frequency of 2.67 Hz corresponds to that of the pedestrian's pace. Consequently, vibrations at the frequencies of the 16th mode of the pedestrian bridge are induced at a pace of 2.70 steps/s.

Regarding the response level induced by a pedestrian walking on the pedestrian bridge, the maximum velocity of the pedestrian bridge induced by a walking pedestrian is less than 0.008 m/s ( $VG = 0.39$ ), which is in the category of 'slightly perceptible'. Therefore, the responses induced by a pedestrian walking on the pedestrian bridge are small.

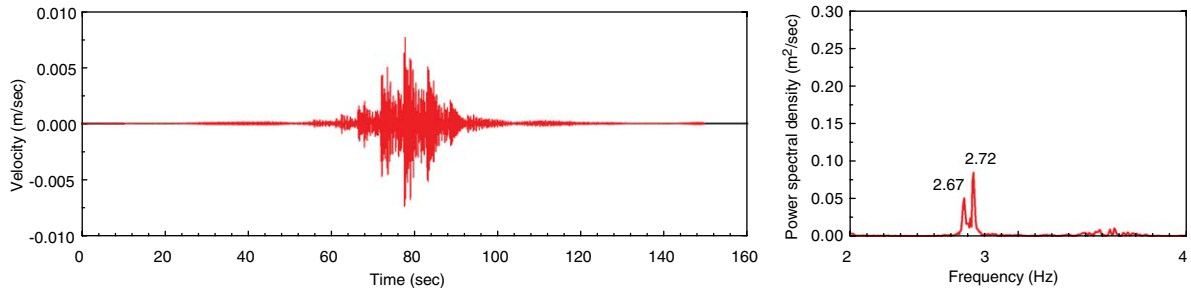


Fig. 18. Time history of velocity and power spectrum of P21061 in the pace of 2.70 steps/s.

## 7. Conclusions

This paper examined the natural vibrations, vehicle- and pedestrian-induced vibrations of the Second Saikai Bridge, which is the first CFT arch highway bridge constructed in Japan. The main findings are as follows:

- (1) The floating mode and the unique antisymmetric mode of the arch bridge are the first two in-plane vibrations of the main bridge, and the first natural frequency of the pedestrian bridge is higher than the lower frequencies of the main bridge.
- (2) The independent pedestrian bridge model can be used to evaluate the natural vibrations of the pedestrian bridge, since the natural frequencies of the pedestrian bridge are separate from those of the main bridge. The influence of the rigidity of the pedestrian bridge on the main bridge is small, since the first in-plane natural frequency is higher than the fundamental frequency of the main bridge.
- (3) The vehicle-induced responses of the main span are small, while the responses in the side spans are larger than those of the main span. The maximum velocity of the side span is about 1.8 cm/s.
- (4) The dynamic response induced by the pedestrian walking on the pedestrian bridge increases when the predominant frequencies of the pedestrian bridge are close to the pace of the pedestrian. However, the response level of the pedestrian bridge is small.

## Acknowledgements

The authors wish to express their gratitude to Chodai Co. Ltd. for providing the materials used in this study.

## References

- [1] C.W. Roeder, B. Cameron, C.B. Brown, Composite action in concrete filled tubes, *Journal of Structural Engineering* 125 (5) (1999) 477–484.

- [2] A.H. Varma, J.M. Ricles, R. Sause, L.W. Lu, Experimental behavior of high strength square concrete-filled steel tube beam-columns, *Journal of Structural Engineering* 128 (3) (2002) 309–318.
- [3] W.C. Clawson, Bridge applications of composite construction in the US, *Structural Engineering in the 21st Century, Proceedings of the Structures Congress*, 1999, pp. 544–547.
- [4] S. Nakamura, New structural forms for steel/concrete composite bridges, *Structural Engineering International* 1 (2000) 45–50.
- [5] Z. Zhen, B. Chen, Q. Wu, Recent development of CFST arch bridge in China, *Proceeding of 6th ASCCS Conference, USA*, 2000, pp.205–212.
- [6] Y. Liu, B. Chen, H. Hikosaka, Recent developments in concrete-filled tubular arch bridge and horizontal swing erection method in China, *Bridge and Foundation Engineering* 33 (2) (1999) 41–44 (in Japanese).
- [7] Q. Wu, B. Chen, K. Takahashi, S. Nakamura, Construction and technical subjects of concrete filled steel tubular arch bridges in China, *Bridge and Foundation Engineering* 35 (10) (2001) 40–45 (in Japanese).
- [8] D. Peng, Q. Wu, K. Takahashi, S. Nakamura, Recent construction and development of long-span bridges in China, *Bridge and Foundation Engineering* 37 (2) (2003) 43–49 (in Japanese).
- [9] Q. Wu, M. Yoshimura, K. Takahashi, S. Nakamura, H. Fujita, K. Furukawa, Vibration and nonlinear seismic analysis of the Second Saikai Bridge-concrete filled tubular (CFT) arch bridge, *Proceedings of the 5th Japan-German Joint Symposium*, Osaka, Japan, 2003, pp.133–142.
- [10] Japan Road Association, *Design Specifications for Highway Bridges, Part I: Steel Bridge*, Maruzen Co., Ltd., Japan, 2002 (in Japanese).
- [11] Q. Wu, K. Takahashi, H. Matsuzaka, B. Chen, S. Nakamura, Study on natural vibrations and nonlinear seismic response of CFT arch bridge constructed in China, *Journal of Constructional Steel* 11 (2003) 177–184 (in Japanese).
- [12] Q. Wu, K. Takahashi, H. Kobayashi, S. Nakamura, Natural vibration properties and nonlinear seismic responses of the Saikai Bridge, *Journal of Constructional Steel* 11 (2003) 185–192 (in Japanese).
- [13] Q. Wu, K. Takahashi, H. Matsuzaka, B. Chen, S. Nakamura, Study on dynamic properties of partially concrete filled steel tubular arch bridge, *Journal of Constructional Steel* 10 (2002) 141–148 (in Japanese).
- [14] T. Okabayashi, Mean square response analysis of highway bridges under a single moving vehicle, *Journal of Structural Mechanics and Earthquake Engineering* 286 (1979) 15–27 (in Japanese).
- [15] J. Xu, T. Okabayashi, Optimal design of a dynamic damper for highway bridge vibration under a moving vehicle, *Proceedings of the Fifth PaciSteel Conference*, Seoul, Korea, 1998, pp. 367–372.
- [16] Q. Wu, K. Takahashi, T. Okabayashi, S. Nakamura, Response characteristics of local vibrations in stay cables on an existing cable-stayed bridge, *Journal of Sound and Vibration* 261 (3) (2003) 403–420.
- [17] R.W. Clough, J. Penzien, *Dynamics of Structure*, McGraw-Hill Kogakusha, 1975.
- [18] Y. Iwatani, Simulation of multidimensional wind fluctuations having any arbitrary power spectra and cross spectra, *Journal of Wind Engineering* 11 (1982) 5–18 (in Japanese).
- [19] ISO (International Organization for Standardization), Proposals for generalized road inputs to vehicles, ISO/TC 108/WG9 Document No.5, 1972.
- [20] T.K. Caughey, Classical normal modes in damped linear dynamic systems, *Journal of Applied Mechanics* 27 (1960) 269–271.
- [21] M. Okatani, B. Chen, Q. Wu, T. Okabayashi, Dynamic behavior of a concrete filled steel tubular arch bridge under traffic road, *Proceedings of Annual Conference of the Japan Society of Civil Engineers*, vol. 56(1) 2001, pp. 288–289.
- [22] T. Kabori, Y. Kajikawa, Ergonomic evaluation methods for bridge vibrations, *Journal of Structural Mechanics and Earthquake Engineering* 230 (1974) 23–31 (in Japanese).
- [23] M. Yoneda, Dynamic response characteristics of the stress ribbon pedestrian bridges due to a walking human and a simplified method for evaluating maximum amplitude of this type of bridges, *Journal of Structural Engineering* 47A (2001) 351–362 (in Japanese).
- [24] M. Yoneda, Relationships between numerical dynamic responses using various human walking force models and full scale measurements of single span pedestrian bridges, *Journal of Structural Engineering* 46A (2000) 439–448 (in Japanese).